

Causal Flow-based Variational Auto-Encoder for Disentangled Causal Representation Learning

DI FAN, School of Mathematical Sciences, Zhejiang University, China

YANNIAN KOU, School of Mathematical Sciences, Zhejiang University, China

CHUANHOU GAO*, School of Mathematical Sciences, Zhejiang University, China

Disentangled representation learning aims to learn low-dimensional representations where each dimension corresponds to an underlying generative factor. While the Variational Auto-Encoder (VAE) is widely used for this purpose, most existing methods assume independence among factors, a simplification that does not hold in many real-world scenarios where factors are often interdependent and exhibit causal relationships. To overcome this limitation, we propose the Disentangled Causal Variational Auto-Encoder (DCVAE), a novel supervised VAE framework that integrates causal flows into the representation learning process, enabling the learning of more meaningful and interpretable disentangled representations. We evaluate DCVAE on both synthetic and real-world datasets, demonstrating its superior ability in causal disentanglement and intervention experiments. Furthermore, DCVAE outperforms state-of-the-art methods in various downstream tasks, highlighting its potential for learning true causal structures among factors.

CCS Concepts: • **Mathematics of computing** → **Variational methods**; • **Computing methodologies** → **Learning latent representations**; **Image representations**.

Additional Key Words and Phrases: variational auto-encoder, disentanglement, representation learning

1 INTRODUCTION

Representation learning aims to learn data representations that simplify the extraction of information for constructing classifiers or predictors [2]. Disentangled representation learning, a key advancement in this field, aims to factorize representations to effectively identify and disentangle latent factors in observed data [29]. Its ability to generate robust and interpretable representations has made it vital in domains such as computer vision and recommendation systems [14, 17, 31, 32, 46, 48, 50].

One widely used framework for learning disentangled representations is the Variational Auto-Encoder (VAE) [23], which has gained significant popularity [10, 26, 39]. The primary focus of existing research is imposing independent constraints on the posterior or aggregated posterior of latent variables z through KL divergence [6–8, 12, 20, 21, 25]. However, these methods assume the independence of generative factors, which often does not align with real-world data, where latent factors are likely to have causal relationships. For example, in a human face image dataset, factors like smiling and mouth opening exhibit a causal relationship: smiling increases the probability of an open mouth, with smiling acting as the causal variable and mouth opening as the effect. Models based on independence assumptions struggle to learn disentangled representations in such cases [45]. To address this, recent approaches have shifted towards causal disentangled representation learning [4, 5, 27, 36, 43, 44], and [29] highlights the importance of supervised learning for disentanglement, suggesting that unsupervised methods are insufficient. Consequently, Structural Causal Models (SCMs) and supervised methods are key to constructing a latent space that causally aligns with ground-truth factors [1, 40, 49]. However, these approaches either rely on pre-existing SCMs to impose causal relationships or focus on modeling the causal structure of

*Corresponding author: Chuanhou Gao

generative factors in specific scenarios. In contrast, we propose incorporating causal relationships into the model using normalizing flows, a recent deep learning technique, thus eliminating the reliance on pre-existing SCMs.

Normalizing flows [33] offer a flexible framework for constructing generative models, ensuring efficient sampling and accurate density estimation. Recently, they have gained prominence in the context of using VAE, where they enhance inference by approximating the posterior distribution more closely to the true data distribution [37]. Among the various types of normalizing flows, autoregressive flows are particularly favored in VAE due to their ability to produce triangular Jacobian matrices [15, 22]. Autoregressive flows have shown promise in learning causal orders between two variables or pairs of multivariate variables, particularly in causal discovery tasks [19]. Wehenkel and Louppe [47] introduced a graphical normalizing flow model, incorporating a conditioner based on an adjacency matrix to improve density estimation from a Bayesian network perspective, though without focusing on causal disentangled representations. Inspired by these advancements, we propose a novel approach, i.e., causal flows based on autoregressive flows. This model not only retains the benefits of traditional autoregressive flows in enhancing VAE’s inference capability but also incorporates causal structural information, enabling VAE to learn causal disentangled representations during inference. This represents the first application of flow models to this task.

In this paper, we introduce causal flows to capture causal relationships among generative factors. We then present a novel VAE-based framework, the Disentangled Causal Variational Auto-Encoder (DCVAE), which integrates VAE with causal flows to learn causal disentangled representations. After encoding the input data with DCVAE’s encoder and processing it through the causal flows, we obtain the causal disentangled representations, which are subsequently fed into the decoder for reconstructing the original images. To increase the flexibility of the prior distribution, we further introduce a conditional prior in DCVAE.

The main contributions can be summarized as follows:

- (1) We introduce causal flows, an enhanced form of autoregressive flows that integrate causal structure information of ground-truth factors to improve representation expressiveness.
- (2) We propose the Disentangled Causal Variational Auto-Encoder (DCVAE), a novel VAE-based framework for learning causal disentangled representations.
- (3) To validate the effectiveness of DCVAE, we conduct extensive experiments on both synthetic and real-world datasets. The results demonstrate that DCVAE successfully generates representations with causal semantics, achieves causal disentanglement, and performs well in intervention experiments, including counterfactual image generation. Additionally, our model excels in sampling efficiency and distributional robustness in downstream tasks.

The remainder of the paper is organized as follows: Section 2 reviews related works, followed by the introduction of preliminaries in section 3. Section 4 presents our proposed causal flows, and section 5 details the overall framework of our model, DCVAE. In section 6, we provide both quantitative and qualitative experiments, offering a comprehensive evaluation of our model’s performance. Finally, section 7 summarizes the contributions of our approach and outlines potential directions for future research.

2 RELATED WORK

2.1 Disentangled Representation Learning

Disentangled representation learning aims to disentangle latent explanatory factors behind the observed data [2]. It assumes that high-dimensional data is generated by low-dimensional, semantically meaningful generative factors, which are called ground-truth factors. Thus, a disentangled

representation is characterized by changes in one dimension being solely caused by one factor of variation in the data. This pursuit, endowed with the ability to generate robust, controllable, and interpretable representations, has emerged as a challenging issue in machine learning.

Generally, variational methods are widely employed for disentangled representation in images, utilizing an encoder-decoder framework to learn mutually independent latent factors. The variational approach employs a standard normal distribution as the prior for latent variables and then uses the variational posterior to approximate the unknown true posterior. By introducing new independent regularization terms into the original loss function, this framework is further extended, giving rise to various algorithms [6–8, 12, 20, 21, 25, 42]. β -VAE [12] imposed a greater weight ($\beta > 1$) on the KL divergence between the variational posterior and prior, thereby employing a modified version of the VAE objective. In β -TCVAE [7], a total correlation penalty was incorporated into the objective to encourage the model to identify statistically independent factors in the data distribution. DIP-VAE [25] introduced a regularizer on the expectation of the approximate posterior over observed data, promoting disentanglement. Unfortunately, Locatello et al. [29] showed that the unsupervised learning of disentangled representations is theoretically impossible from observations without inductive biases. Therefore, several weakly supervised or supervised methods were proposed [3, 13, 30, 41]. For instance, Locatello et al. [30] explored the task of learning disentangled representations from pairs of non-i.i.d. observations, where these observations share an unknown, random subset of factors of variation. They also investigated the impact of different supervision modalities. Furthermore, Khemakhem et al. [18] introduced a conditional VAE, assuming that latent variables are conditionally independent given some additionally observed variables. The latent variable model they proposed, particularly VAE, generated a provable disentangled representation under appropriate conditions.

However, the most popular existing methods for disentanglement fail to effectively learn disentangled representations for data with strongly correlated factors, a scenario commonly encountered in real-world situations [40, 45].

2.2 Causal Representation Learning

Recognizing the limitations of the aforementioned methods in addressing general scenarios, there has been growing interest in achieving causal disentangled representations through VAE. However, research in this area remains relatively limited.

Schölkopf [38] highlighted the importance of causal disentangled representations, providing a conceptual foundation. The disentangled causal mechanisms explored in Suter et al. [44] and Reddy et al. [36] assume conditional independence of underlying factors given a shared confounder. This assumption imposes strict constraints on the latent structure of generative factors, excluding cases where real factors may have causal relationships with one another. For models that do not impose causal graph constraints, supervised methods are often used. Locatello et al. [29] emphasized the importance of supervised learning for disentanglement, suggesting that unsupervised methods are insufficient. Consequently, Structural Causal Models (SCMs) and supervised techniques play a critical role in constructing a latent space that causally aligns with ground-truth factors [1, 40, 49]. Yang et al. [49] proposed an SCM layer to model the causal generative mechanisms of data, extending iVAE [18] by using a conditional prior based on ground-truth factors, operating in a fully supervised manner. Similarly, DEAR [40] utilized an SCM to construct the prior distribution in a weakly supervised setting. An et al. [1] emphasized the importance of training a disentangled decoder and introduced a supervised learning approach for VAE. In our work, we also leverage supervision signals from concept labels. We believe this supervised approach is both feasible and applicable to real-world datasets. For example, in the case of human face datasets, features such as gender and smiling status can be easily extracted from raw data.

Other models have also imposed structure on the latent space of VAEs. For example, Graph VAE [11] applied a chained structure and imposed a structural causal model (SCM) on the VAE’s latent space. However, the main goal of Graph VAE is to enhance VAE’s expressive power, rather than specifically focusing on disentangling latent causal factors. Several other methods have been proposed for learning causal disentangled representations, extending beyond generative models like VAE [24, 38, 44]. However, unlike these methods, our model introduces causal flows within VAE, resulting in a significantly different model structure.

Relatively speaking, our proposed model is designed to handle general scenarios where generative factors exhibit more complex causal relationships. Unlike SCM-based methods, we utilize the strengths of flow models to achieve disentanglement. This approach not only leverages the flexible fitting capacity of flow models but also benefits from the causal insights offered by SCMs. In other words, our model integrates causal information while enhancing the expressive power of VAE’s inference process. Importantly, our primary focus is on representation learning, with an emphasis on the disentangled representations generated by the encoder. To the best of our knowledge, our model is the first VAE-based framework to achieve causal disentanglement without relying on complex SCMs. Furthermore, it successfully learns causal disentangled representations without imposing constraints on the causal graph of generative factors.

3 PRELIMINARIES

3.1 Variational Auto-Encoder

Let $\{\mathbf{x}^{(j)}\}_{j=1}^N$ denote i.i.d training data, $\mathbf{x} \in \mathbb{R}^n$ be the observed variables and $\mathbf{z} \in \mathbb{R}^d$ be the latent variables. The dataset \mathcal{X} has an empirical data distribution denoted as $q_{\mathcal{X}}$. The *generative model* defined over \mathbf{x} and \mathbf{z} is $p_{\theta}(\mathbf{x}, \mathbf{z}) = p(\mathbf{z})p_{\theta}(\mathbf{x}|\mathbf{z})$, where θ is the parameter of the *decoder*. Typically, $p(\mathbf{z}) = \mathcal{N}(\mathbf{0}, \mathbf{I})$, $p_{\theta}(\mathbf{x}|\mathbf{z}) = \mathcal{N}(f_{\theta}(\mathbf{z}), \sigma^2\mathbf{I})$, where $f_{\theta}(\mathbf{z})$ is a neural network. The marginal likelihood $p_{\theta}(\mathbf{x}) = \int p_{\theta}(\mathbf{x}, \mathbf{z})d\mathbf{z}$ is intractable to maximize. Therefore, VAE [23] introduces a parametric *encoder* $q_{\eta}(\mathbf{z}|\mathbf{x}) = \mathcal{N}(\mu_{\eta}(\mathbf{x}), \text{diag}(\sigma_{\eta}^2(\mathbf{x})))$, also called an *inference model*, to obtain the variational lower bound on the marginal log-likelihood, i.e., the Evidence Lower Bound (ELBO):

$$\begin{aligned} \text{ELBO}(\boldsymbol{\eta}, \boldsymbol{\theta}) &= \mathbb{E}_{q_{\mathcal{X}}} [\log p_{\theta}(\mathbf{x}) - D_{\text{KL}}(q_{\eta}(\mathbf{z}|\mathbf{x})\|p_{\theta}(\mathbf{z}|\mathbf{x}))] \\ &= \mathbb{E}_{q_{\mathcal{X}}} [\mathbb{E}_{q_{\eta}(\mathbf{z}|\mathbf{x})} (\log p_{\theta}(\mathbf{x}, \mathbf{z}) - \log q_{\eta}(\mathbf{z}|\mathbf{x}))] \\ &= \mathbb{E}_{q_{\mathcal{X}}} [\mathbb{E}_{q_{\eta}(\mathbf{z}|\mathbf{x})} \log p_{\theta}(\mathbf{x}|\mathbf{z}) - D_{\text{KL}}(q_{\eta}(\mathbf{z}|\mathbf{x})\|p(\mathbf{z}))] \end{aligned} \quad (1)$$

where $\boldsymbol{\eta}$ is the parameter of the *encoder*. As can be seen from Eq. (1), maximizing $\text{ELBO}(\boldsymbol{\eta}, \boldsymbol{\theta})$ will simultaneously maximize $\log p_{\theta}(\mathbf{x})$ and minimize KL divergence $D_{\text{KL}}(q_{\eta}(\mathbf{z}|\mathbf{x})\|p_{\theta}(\mathbf{z}|\mathbf{x})) \geq 0$. Therefore, we wish $q_{\eta}(\mathbf{z}|\mathbf{x})$ to be flexible enough to match the true posterior $p_{\theta}(\mathbf{z}|\mathbf{x})$. At the same time, based on the third line of Eq. (1), which is often used as the objective function of VAE, we require that $q_{\eta}(\mathbf{z}|\mathbf{x})$ is efficiently computable, differentiable, and sampled from.

3.2 Autoregressive Normalizing Flows

Normalizing flows [37] are effective solutions to the issues mentioned above. The flows construct flexible posterior distribution through expressing $q_{\eta}(\mathbf{z}|\mathbf{x})$ as an expressive invertible and differentiable mapping \mathbf{g} of a random variable with a relatively simple distribution, such as an isotropic normal. Typically, \mathbf{g} is obtained by composing a sequence of invertible and differentiable transformations $\mathbf{g}^{(1)}, \mathbf{g}^{(2)}, \dots, \mathbf{g}^{(K)}$, i.e., $\mathbf{g} = \mathbf{g}^{(K)} \circ \dots \circ \mathbf{g}^{(1)}$, $\mathbf{g}^{(k)} : \mathbb{R}^{d+n} \rightarrow \mathbb{R}^d, \forall k = 1 \dots K$. If we define the initial random variable (the output of encoder) as $\mathbf{z}^{(0)}$ and the final output random variable as $\mathbf{z}^{(K)}$, then $\mathbf{z}^{(k)} = \mathbf{g}^{(k)}(\mathbf{z}^{(k-1)}, \mathbf{x}), \forall k$. In this case, we can use \mathbf{g} to obtain the conditional probability

density function of $\mathbf{z}^{(K)}$ by applying the general probability-transformation formula [33]:

$$q_{\eta}(\mathbf{z}^{(K)}|\mathbf{x}) = q_{\eta}(\mathbf{z}^{(0)}|\mathbf{x}) \left| \det J_{\mathbf{g}(\mathbf{z}^{(0)},\mathbf{x})} \right| \quad (2)$$

where $\det J_{\mathbf{g}(\mathbf{z}^{(0)},\mathbf{x})}$ is the Jacobian determinant of \mathbf{g} with respect to $\mathbf{z}^{(0)}$.

Autoregressive flows are one of the most popular normalizing flows [15, 22, 33]. By carefully designing the function \mathbf{g} , the Jacobian matrix in Eq. (2) becomes a lower triangular matrix. For illustration, we will only use a single-step flow with notation \mathbf{g} . Multi-layer flows are simply the composition of the function represented by a single-step flow, as mentioned earlier. And we will denote the input to the function \mathbf{g} as \mathbf{z} and its output as $\tilde{\mathbf{z}}$. In the autoregressive flows, \mathbf{g} has the following form:

$$\begin{aligned} \tilde{\mathbf{z}} = \mathbf{g}(\mathbf{z}, \mathbf{x}) &= [g_1(\mathbf{z}_1; \mathbf{h}_1) \dots g_d(\mathbf{z}_d; \mathbf{h}_d)]^T \\ \text{where } \mathbf{h}_i &= \mathbf{c}_i(\tilde{\mathbf{z}}_{<i}, \mathbf{x}) \end{aligned} \quad (3)$$

where g_i , an invertible function of input \mathbf{z}_i , is termed as a **transformer**. Here \mathbf{z}_i stands for the i -th element of vector \mathbf{z} , and \mathbf{c}_i is the i -th **conditioner**, a function of the first $i - 1$ elements of $\tilde{\mathbf{z}}$, which determines part of parameters of the transformer g_i . We use neural networks to fit \mathbf{c} .

4 CAUSAL FLOWS

In this section, we propose an extension to the autoregressive flows by incorporating an adjacency matrix A . The extended flows still involve functions with tractable Jacobian determinants.

In autoregressive flows, causal order is established among variables $\tilde{\mathbf{z}}_1, \dots, \tilde{\mathbf{z}}_d$. Given the causal graph of the variables $\tilde{\mathbf{z}}_1, \dots, \tilde{\mathbf{z}}_d$, let $A \in \mathbb{R}^{d \times d}$ denote its corresponding binary adjacency matrix, $A_{i,:}$ is the row vector of A and $A_{i,j}$ is nonzero only if $\tilde{\mathbf{z}}_j$ is the parent node of $\tilde{\mathbf{z}}_i$, then A corresponding to the causal order in autoregressive flows is a full lower-triangular matrix. The conditioner can be written in the form of $\mathbf{c}_i(\tilde{\mathbf{z}} \circ A_{i,:}, \mathbf{x})$, where \circ is the element-wise product. If we utilize prior knowledge about the true causal structure among variables, i.e., if a certain causal structure among variables is known, then A is still a lower triangular matrix, but some of its entries are set to 0. We can integrate such A into the conditioner to include causal structure information in the model, which is also denoted as $\mathbf{c}_i(\tilde{\mathbf{z}} \circ A_{i,:}, \mathbf{x})$. We will refer to it as the **causal conditioner** in the following.

We define autoregressive flows that use the causal conditioner as **Causal Flows**. The transformer can be any invertible function, and we focus on affine transformer, which is one of the simplest transformers. Therefore, causal flows \mathbf{g} can be formulated as follows:

$$\tilde{\mathbf{z}}_i = g_i(\mathbf{z}_i; \mathbf{h}_i) = \mathbf{z}_i \exp(s_i(\tilde{\mathbf{z}} \circ A_{i,:}, \mathbf{x})) + t_i(\tilde{\mathbf{z}} \circ A_{i,:}, \mathbf{x}) \quad (4)$$

where $\mathbf{s} = [s_1, \dots, s_d]^T \in \mathbb{R}^d$ and $\mathbf{t} = [t_1, \dots, t_d]^T \in \mathbb{R}^d$ are defined by the conditioner, i.e., $\mathbf{h}_i = \{s_i, t_i\}$, and s_1 and t_1 are constants.

Given that the derivative of the transformer with respect to \mathbf{z}_i is $\exp(s_i(\tilde{\mathbf{z}} \circ A_{i,:}, \mathbf{x}))$ and A is lower-triangular, the log absolute Jacobian determinant is:

$$\log |\det J_{\mathbf{g}(\mathbf{z},\mathbf{x})}| = \sum_{i=1}^d \log \exp(s_i(\tilde{\mathbf{z}} \circ A_{i,:}, \mathbf{x})) \quad (5)$$

$$= \sum_{i=1}^d s_i(\tilde{\mathbf{z}} \circ A_{i,:}, \mathbf{x}) \quad (6)$$

Now, we are able to derive the log probability density function of $\tilde{\mathbf{z}}$ using the following expression:

$$\log q_{\eta}(\tilde{\mathbf{z}}|\mathbf{x}) = \log q_{\eta}(\mathbf{z}|\mathbf{x}) - \sum_{i=1}^d s_i(\tilde{\mathbf{z}} \circ A_{i,:}, \mathbf{x}) \quad (7)$$

Causal flows will not only empower our model to incorporate causal structure information but also through the utilization of flow model characteristics, enhance the expressive capacity of the learned representations. This augmentation, consequently, enriches the information encoded in the learned representations, thereby improving the overall proficiency of our model.

It is worth noting that the computation of autoregressive flows in Eq. (3) needs to be performed sequentially, meaning that $\tilde{\mathbf{z}}_{<i}$ must be calculated before $\tilde{\mathbf{z}}_i$. Due to the sampling requirement in VAE, this approach may not be computationally efficient. However, in causal disentanglement applications of VAE, the number of factors of interest is often relatively small. Additionally, we've found that using a single layer of causal flows and lower-dimensional latent variables is enough to lead to better results, so the computational cost of the model is not significantly affected by sequential sampling.

5 THE PROPOSED MODEL

This section focuses on addressing the issue of causal disentanglement in VAE. First, we introduce some notations. We denote $\xi \in \mathbb{R}^m$ as the underlying ground-truth factors of interest for data \mathbf{x} , with distribution p_{ξ} . For each underlying factor ξ_i , we denote \mathbf{y}_i as some continuous or discrete annotated observation satisfying $\xi_i = \mathbb{E}(\mathbf{y}_i|\mathbf{x})$, where the superscript i still denotes the i -th element of each vector. Let $\mathcal{D} = \{(\mathbf{x}^{(j)}, \mathbf{y}^{(j)}, \mathbf{u}^{(j)})\}_{j=1}^N$ denotes a labeled dataset, where $\mathbf{u}^{(j)} \in \mathbb{R}^k$ is the additional observed variable. Depending on the context, the variable \mathbf{u} can take on various meanings, such as serving as the time index in a time series, a class label, or another variable that is observed concurrently [16]. When \mathbf{u} is the ground-truth factor \mathbf{y} , $\xi_i = \mathbb{E}(\mathbf{y}_i|\mathbf{x}, \mathbf{u})$, which is obviously true. Otherwise, when \mathbf{u} is not the ground-truth factor \mathbf{y} , i.e., when \mathbf{y} and \mathbf{u} are entirely unrelated, $\xi_i = \mathbb{E}(\mathbf{y}_i|\mathbf{x}) = \mathbb{E}(\mathbf{y}_i|\mathbf{x}, \mathbf{u})$. Thus, we obtain $\xi_i = \mathbb{E}(\mathbf{y}_i|\mathbf{x}, \mathbf{u})$, where $i = 1, \dots, m$. We will view the encoder and flows as a unified stochastic transformation E , with the learned representation $\tilde{\mathbf{z}}$ as its final output, i.e., $\tilde{\mathbf{z}} = E(\mathbf{x}, \mathbf{u})$. Additionally, in the stochastic transformation $E(\mathbf{x}, \mathbf{u})$, we use $\bar{E}(\mathbf{x}, \mathbf{u})$ to denote its deterministic part, i.e., $\bar{E}(\mathbf{x}, \mathbf{u}) = \mathbb{E}(E(\mathbf{x}, \mathbf{u})|\mathbf{x}, \mathbf{u})$.

Now, we adopt the definition of causal disentanglement as follows:

Definition 5.1 (Disentangled representation [40]). Considering the underlying factor $\xi \in \mathbb{R}^m$ of data \mathbf{x} , E is said to learn a disentangled representation with respect to ξ if there exists a one-to-one function r_i such that $\bar{E}(\mathbf{x}, \mathbf{u})_i = r_i(\xi_i), \forall i = 1, \dots, m$.

The purpose of this definition is to guarantee some degree of alignment between the latent variable $E(\mathbf{x})$ and the underlying factor ξ in the model.

We now proceed to present the full probabilistic formulation of DCVAE. The model's structure is depicted in Figure 1. The conditional generative model is defined as follows:

$$p_{\theta}(\mathbf{x}, \tilde{\mathbf{z}}|\mathbf{u}) = p_{\mathbf{f}}(\mathbf{x}|\tilde{\mathbf{z}}, \mathbf{u})p_{\mathbf{T}, \lambda}(\tilde{\mathbf{z}}|\mathbf{u}) \quad (8)$$

$$p_{\mathbf{f}}(\mathbf{x}|\tilde{\mathbf{z}}, \mathbf{u}) = p_{\mathbf{f}}(\mathbf{x}|\tilde{\mathbf{z}}) = p_{\zeta}(\mathbf{x} - \mathbf{f}(\tilde{\mathbf{z}})) \quad (9)$$

with

$$p_{\mathbf{T}, \lambda}(\tilde{\mathbf{z}}|\mathbf{u}) = \begin{cases} \frac{Q(\tilde{\mathbf{z}}_{\leq m})e^{<T(\tilde{\mathbf{z}}_{\leq m}), \lambda(\mathbf{u})>}}{Z(\mathbf{u})} \\ \mathcal{N}(\mathbf{0}_{(d-m) \times 1}, \mathbf{I}_{(d-m) \times (d-m)}) \end{cases} \quad (10)$$

where $\theta = (\mathbf{f}, \mathbf{T}, \lambda) \in \Theta$ are model parameters, $p_{\mathbf{T}, \lambda}(\tilde{\mathbf{z}}|\mathbf{u}) > 0$ is almost surely $\forall (\tilde{\mathbf{z}}, \mathbf{u}) \in \tilde{\mathbf{Z}} \times \mathbf{U}$ with

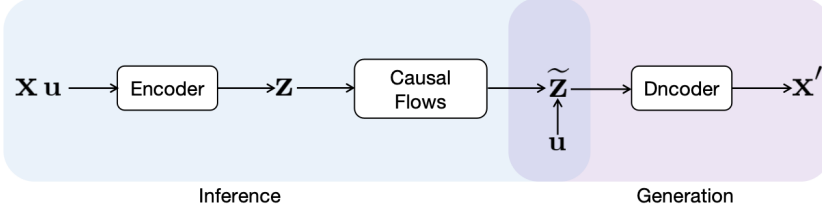


Fig. 1. Model structure of DCVAE.

$\tilde{\mathbf{Z}}$ and \mathbf{U} to be compact Hausdorff spaces. Eq. (8) describes the process of generating \mathbf{x} from $\tilde{\mathbf{z}}$. Eq. (9) indicates that $\mathbf{x} = \mathbf{f}(\tilde{\mathbf{z}}) + \zeta$, where $p_{\zeta}(\zeta) = \mathcal{N}(\mathbf{0}, \mathbf{I})$ and the decoder $\mathbf{f}(\tilde{\mathbf{z}})$ is assumed to be an invertible function approximated by a neural network. In Eq. (10), the first equation is used for the first m dimensions of $\tilde{\mathbf{z}}$ while the second one serves for the remaining $d - m$ dimensions to capture other non-interest factors for generation; $\mathbf{T} : \mathbb{R}^d \rightarrow \mathbb{R}^{d \times l}$ is the sufficient statistic, $\boldsymbol{\lambda} : \mathbb{R}^k \rightarrow \mathbb{R}^{d \times l}$ is the corresponding parameter, $Q : \mathbb{R}^d \rightarrow \mathbb{R}$ is the base measure, $Z(\mathbf{u})$ is the normalizing constant and $\langle \cdot, \cdot \rangle$ denotes the dot product. If $d = m$, we will only use the conditional prior in the first line of (10). When causal relationships exist among the generative factors of data \mathbf{x} , indicating their non-mutual independence, incorporating information \mathbf{u} alters the prior distribution from a factorial distribution to a distribution that better matches the real-world situation.

We define the inference model that utilizes causal flows as follows:

$$q_{\eta}(\mathbf{z}|\mathbf{x}, \mathbf{u}) = q_{\epsilon}(\mathbf{z} - \boldsymbol{\phi}(\mathbf{x}, \mathbf{u})) \quad (11)$$

$$\mathbf{z} \sim q_{\eta}(\mathbf{z}|\mathbf{x}, \mathbf{u}) \quad (12)$$

$$\tilde{\mathbf{z}} = \mathbf{g}(\mathbf{z}, \mathbf{x}) \quad (13)$$

$$q_{\eta, \gamma}(\tilde{\mathbf{z}}|\mathbf{x}, \mathbf{u}) = q_{\eta}(\mathbf{z}|\mathbf{x}, \mathbf{u}) \prod_{i=1}^d \exp(-s_i(\tilde{\mathbf{z}} \circ A_{i, \cdot}, \mathbf{x})) \quad (14)$$

where $\boldsymbol{\gamma} = (\mathbf{s}, \mathbf{t}, A) \in \Gamma$ denotes parameters of causal flows. Eq. (11) indicates that $\mathbf{z} = \boldsymbol{\phi}(\mathbf{x}, \mathbf{u}) + \epsilon$, where the probability density of ϵ is $q_{\epsilon}(\epsilon) = \mathcal{N}(\mathbf{0}, \mathbf{I})$ and $\boldsymbol{\phi}(\mathbf{x}, \mathbf{u})$ denotes the encoder. Eq. (12) and (13) describe the process of transforming the original encoder output \mathbf{z} into the final latent variable representation $\tilde{\mathbf{z}}$ by using causal flows. Eventually, the posterior distribution obtained by the inference model is represented by Eq. (14). So the parameters of stochastic transformation $E(\mathbf{x}, \mathbf{u})$ are $\boldsymbol{\eta}$ and $\boldsymbol{\gamma}$, which we denote as $E_{\boldsymbol{\eta}, \boldsymbol{\gamma}}(\mathbf{x}, \mathbf{u})$.

Now the dataset \mathcal{X} has an empirical data distribution denoted by $q_{\mathcal{X}}(\mathbf{x}, \mathbf{u})$. Our goal is to maximize the variational lower bound on the marginal likelihood $p_{\theta}(\mathbf{x}|\mathbf{u})$. The labels \mathbf{y} represent the ground-truth latent factors. We introduce a regularization term in the objective function to encourage consistency between $\boldsymbol{\xi}$ and $E(\mathbf{x}, \mathbf{u})$. The loss function of DCVAE is formulated as follows:

$$\begin{aligned} \mathcal{L}(\boldsymbol{\eta}, \boldsymbol{\gamma}, \boldsymbol{\theta}) &= -\text{ELBO}(\boldsymbol{\phi}, \boldsymbol{\gamma}, \boldsymbol{\theta}) + \beta_{sup} \mathcal{L}_{sup}(\boldsymbol{\eta}, \boldsymbol{\gamma}) \\ &= -\mathbb{E}_{q_{\mathcal{X}}} [\mathbb{E}_{q_{\eta, \gamma}(\tilde{\mathbf{z}}|\mathbf{x}, \mathbf{u})} \log p_{\mathbf{f}}(\mathbf{x}|\tilde{\mathbf{z}}, \mathbf{u})] \\ &\quad - D_{\text{KL}}(q_{\eta, \gamma}(\tilde{\mathbf{z}}|\mathbf{x}, \mathbf{u}) \| p_{\mathbf{T}, \boldsymbol{\lambda}}(\tilde{\mathbf{z}}|\mathbf{u})) \\ &\quad + \beta_{sup} \mathbb{E}_{(\mathbf{x}, \mathbf{y}, \mathbf{u})} [l_{sup}(\boldsymbol{\eta}, \boldsymbol{\gamma})] \end{aligned} \quad (15)$$

where $\beta_{sup} > 0$ is a hyperparameter, $l_{sup}(\boldsymbol{\eta}, \boldsymbol{\gamma}) = \sum_{i=1}^m (\mathbf{y}_i - \bar{E}_{\boldsymbol{\eta}, \boldsymbol{\gamma}}(\mathbf{x}, \mathbf{u})_i)^2$ is the Mean Squared Error if \mathbf{y}_i is the continuous observation, and $l_{sup}(\boldsymbol{\eta}, \boldsymbol{\gamma}) = \sum_{i=1}^m -\mathbf{y}_i \log \sigma(\bar{E}_{\boldsymbol{\eta}, \boldsymbol{\gamma}}(\mathbf{x}, \mathbf{u})_i) - (1 - \mathbf{y}_i) \log (1 - \sigma(\bar{E}_{\boldsymbol{\eta}, \boldsymbol{\gamma}}(\mathbf{x}, \mathbf{u})_i))$ is the cross-entropy loss if \mathbf{y}_i is the binary label. The loss term \mathcal{L}_{sup} aligns the

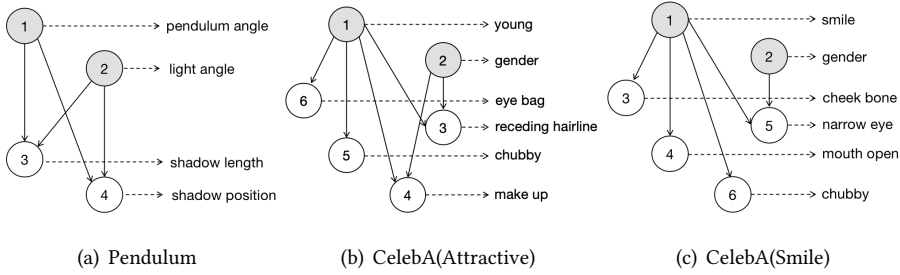


Fig. 2. Causal graphs of Pendulum and CelebA. The gray circles represent the causal variables in the graphs. In Figures (a), (b), and (c), we label the underlying factors we are interested in each dataset.

factor of interest $\xi \in \mathbb{R}^m$ with the first m dimensions of the latent variable \tilde{z} , in order to satisfy the Definition 5.1 [30, 40].

As demonstrated in [40], even under the supervision of latent variables, previously employed disentangled representation learning methods, based on the assumption of independent priors, fail to achieve true disentanglement when causal relationships exist among the latent factors of interest (i.e., the disentanglement identifiability discussed earlier in Definition 5.1). To address the identifiability issue raised in [40], we incorporate additional information, denoted as \mathbf{u} . We utilize this additional information in two ways. First, we propose integrating it into conditional priors to regularize the learned posterior of \mathbf{z} . This regularization allows us to focus on priors that are more aligned with the true generating factors of interest. Moreover, the use of these conditional priors ensures that the learned representation is indeed disentangled, as defined in Definition 5.1, thus addressing the identifiability concerns, with the proof being similar to that in [40]. Second, in real-world experiments, if we take \mathbf{u} as concept labels, it will function as regularization terms, thereby constraining the latent variable information, i.e., as \mathbf{y} . As highlighted in section 2.2, existing methods primarily focus on supervised models, which are readily implementable in practice. This highlights the practicality and real-world applicability of our approach.

6 EXPERIMENTS

In this section, we empirically evaluate DCVAE, demonstrating that the learned representation is causally disentangled. This capability will enable the model to perform across various tasks effectively.

6.1 Datasets

We utilize the same datasets from Shen et al. [40], where the underlying generative factors are causally related. The synthetic dataset is Pendulum, with four continuous factors whose causal graph of the factors is shown in Figure 2(a). We generate the pendulum dataset using the synthetic simulators mentioned in Yang et al. [49]. The training and testing sets consist of 5847 and 1461 samples, respectively. The real human face dataset is CelebA [28], with 40 discrete labels. We consider two sets of causally related factors named CelebA(Attractive) and CelebA(Smile) with causal graphs also depicted in Figure 2(b) and 2(c). We set the values of features to $[-1, 0]$. The training and testing sets consist of 162770 and 19962 samples, respectively. In the datasets, \mathbf{x} represents the sample, \mathbf{y} denotes the true label information of the generating factors, and \mathbf{u} is the additional observed variable, which we have designated as label information for the experiments. All the images are resized to $64 \times 64 \times 3$ resolution.

6.2 Experimental Settings and Baselines

We present the main settings used in our experiments. Our experiments on Pendulum utilize one NVIDIA GeForce RTX 2080ti GPU, while experiments on CelebA use one NVIDIA GeForce RTX 3080 GPU. To train DEAR, we use two NVIDIA GeForce RTX 2080ti GPUs.

6.2.1 DCVAE. In DCVAE, regarding the setting of conditional prior of DCVAE, since it is generally difficult to directly fit the exponential family of distributions, we use a special form of exponential distribution, namely the Gaussian distribution in our experiments. For simplicity, we adopt a factorial distribution, as described in Khemakhem et al. [18] and Yang et al. [49]. However, unlike them, we set the *mean* and *variance* as learnable parameters for training, which enhances the flexibility of the prior distribution. In the implementation of the supervised loss for Pendulum, the factors' labels are resized to $[-1, 1]$ because they are continuous, and Mean Squared Error (MSE) is employed as the loss function \mathcal{L}_{sup} . For CelebA, where the factors' labels are binary, we map -1 to 0 and utilize cross-entropy loss. Since we incorporate additional information \mathbf{u} relevant to the true concept labels as the supervision signal in our experiment, the encoder in DCVAE only takes \mathbf{x} as input and does not use \mathbf{u} to avoid information leakage. The comprehensive details of the network architectures and hyperparameters are given in Appendix A.

6.2.2 Baseline models. We compare our method with several state-of-the-art VAE-based models for disentanglement [29], including β -VAE [12], β -TCVAE [7], DEAR [40] and VAE [23]. We also investigate prior information with limited understanding of causal graph structures. Specifically, DCVAE-SP represents a DCVAE trained using the given super-graph of the true graph (i.e., Figure 7), rather than the full graph. In this context, β -VAE and β -TCVAE stand out as the most representative VAE-based disentanglement models, imposing independent constraints on the posterior and utilizing total correlation to encourage independence among aggregated posteriors, respectively. Currently, the most advanced causal disentanglement model based on VAE is DEAR. Therefore, overall, the selected comparison models are all representative. We use the same conditional prior and loss term with labeled data for each of these methods as in DCVAE, except that DEAR's prior is SCM prior. Furthermore, apart from models that specifically choose the architecture of encoder and decoder, we employ identical encoder and decoder structures for the baselines. The implementations of β -TCVAE and DEAR are each associated with publicly available source codes, which can be found at <https://github.com/AntixK/PyTorch-VAE> and <http://jmlr.org/papers/v23/21-0080.html>. It is worth noting that we did not compare our results with the model in Yang et al. [49]. Firstly, due

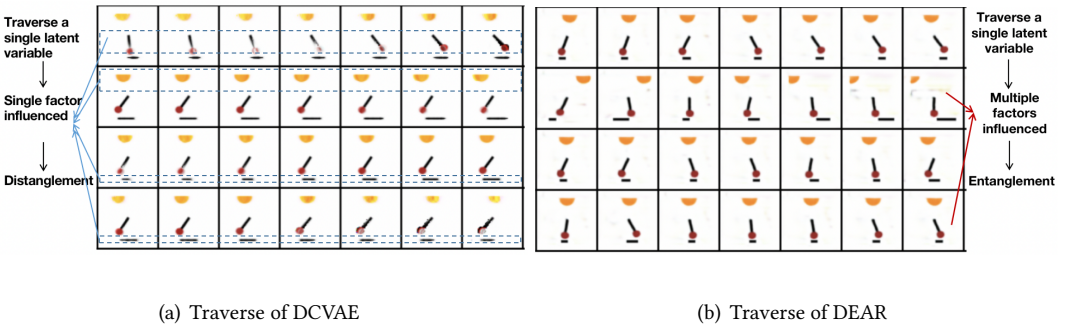


Fig. 3. Results of traverse experiments on Pendulum. Each row corresponds to a variable that we traverse on, specifically, pendulum angle, light angle, shadow length, and shadow position.

to the presence of a Mask layer in its decoder, it is not possible to observe changes in individual factors when traversing each dimension of the learned representation. Secondly, the latent variable dimension in the model corresponds to the number of interested latent factors, which, when applied to real-world datasets, may not enable the latent layer to capture all the generative factors of the images, thereby failing to ensure a one-to-one correspondence between latent units and generative factors, and consequently, not achieving causal disentanglement. Additionally, regarding the pendulum dataset, to ensure model performance, the authors of Yang et al. [49] assigned a multidimensional vector with a dimension of 4 to each latent factor which could not be aligned with our model. Consequently, due to the issue with the dimension of latent variables in their model, we did not perform a comparison. In contrast, DEAR, as a VAE-based causal disentanglement model, is more reasonable. To ensure a fair comparison with equal amounts of supervised information, for each of these methods we use the same conditional prior and loss term as in DCVAE.

6.3 Experimental Results

Now, we proceed to evaluate our method through both qualitative and quantitative experiments and provide an analysis of the corresponding experimental results.

6.3.1 Causal Disentangled Representations. To qualitatively verify that DCVAE indeed learns causal disentangled representations, we conduct intervention experiments.

Intervention experiments involve performing the "do-operation" in causal inference [34]. Taking a single-step causal flow as an example, we demonstrate step by step how our model performs "do-operation". First, given a trained model, we input the sample x into the inference model, obtaining an output \tilde{z} . Assuming we wish to perform the "do-operation" on \tilde{z}_i , i.e., $do(\tilde{z}_i = c)$, we follow the approach in Khemakhem et al. [19] by treating Eq. (4) as SEMs. Specifically, we set the input and output of \tilde{z}_i to the control value c , while other values are computed iteratively from input to output. Finally, the resulting \tilde{z} is decoded to generate the desired image, which corresponds to generating images from the interventional distribution of \tilde{z} .

We perform intervention experiments by applying the "do-operation" to $m - 1$ variables in the first m dimensions of the latent variables, resulting in the change of only one variable. This operation, which has been referred to as "traverse", aims to test the disentanglement of our model [40]. Figures 3 and 4 show the experimental results of the DCVAE and DEAR on Pendulum and CelebA(Smile). We observe that when traversing a latent variable dimension, DCVAE has almost



Fig. 4. Results of traverse experiments on CelebA(Smile). Each row corresponds to a variable that we traverse on, specifically, smile, gender, cheek bone, mouth open, narrow eye and chubby.

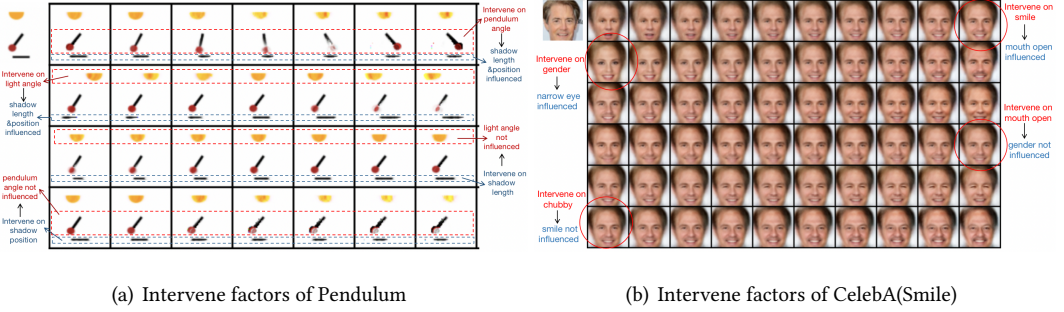


Fig. 5. Results of intervention on only one variable for both Pendulum and CelebA(Smile). The image in the upper left corner of (a) and (b) are the test data we consider respectively.

only one factor changing, while DEAR has multiple factors changing. This is clearly shown by comparing "traverse" results of the third row for shadow length in Figures 3(a) and 3(b), as well as the second row for gender in Figures 4(a) and 4(b). Therefore, our model performs better in achieving causal disentanglement.

To demonstrate our model's capability to perform interventions hence generating new images beyond the dataset, we further conduct "do-operations" on individual latent variables. Figure 5 illustrates these operations, with each row representing an intervention on a single dimension. In Figure 5(a), we observe that intervening on the pendulum angle and light angle produces changes in shadow length in accordance with physical principles. However, intervening on shadow length has minimal impact on these two factors. Similarly, as illustrated in Figure 5(b), intervening on gender influences narrow eye appearance, but the reverse is not true. This demonstrates that intervening on causal factors affects the resulting effects, but not the other way around. Hence, our latent variables have effectively learned factor representations, attributed to the design of the causal flows, which incorporate A . Additional traversal and intervention results are presented in Appendix B.

The clarity of the images generated by our model, as shown in Figure 3(a), is somewhat lower compared to those produced by An et al. [1]. However, the images generated from the CelebA(Smile) dataset, as shown in Figure 4(a), are clearer than those in Figure 3(a). One possible solution is to increase the sampling size of the datasets used in future practical applications as much as possible when using the model. On the other hand, the Causally Disentangled Generation (CDG) model by An et al. [1] significantly enhances the VAE decoder, resulting in clearer counterfactual images by accurately reflecting the data generation process. In contrast, our model focuses on optimizing the encoder to learn disentangled representations and relies on the decoder to generate high-quality images. Therefore, to address the issue of image clarity, we will explore methods to improve our model's performance, including integrating techniques from An et al. [1] or other methods to enhance the decoder's performance. This would help ensure higher image quality in our model's output. In summary, addressing this challenge will be a key focus of our future work.

6.3.2 Downstream tasks. To quantitatively illustrate the benefits of causal disentangled representations, we consider its impact on downstream tasks in terms of sample efficiency and distributional robustness. We introduce two downstream prediction tasks to compare our model with baseline models. First, for Pendulum, we normalize factors to $[-1, 1]$ during preprocessing. Then, we manually create a classification task: if $pendulum\ angle > 0$ and $light\ angle > 0$, the target label $y = 1$; otherwise, $y = 0$. For the CelebA(Attractive), we adopt the same classification task as presented

in [40]. We employ multilayer perceptron (MLP) to train classification models, where both the training and testing sets consist of the latent representations \tilde{z} and their corresponding labels y .

Sample Efficiency: The experimental results are presented in Table 1. We adopt the statistical efficiency score defined in Locatello et al. [29] as a measure of sample efficiency, which is defined as the classification accuracy of 100 test samples divided by the number of all (Pendulum)/10,000 test samples (CelebA). Table 1 shows that DCVAE achieves the best sample efficiency on both datasets. DCVAE-SP exhibits slightly inferior performance compared to DCVAE because the causal information input into DCVAE-SP is weaker than that in DCVAE, which contributes to its reduced performance, but it remains competitive when compared to other baseline methods. Hence, while the model’s optimal performance is achieved by integrating information from the full graph, causal flows can still contribute with slightly diminished effectiveness in the case of the super-graph. This emphasizes the significance of incorporating causal flow in our model. We attribute the superiority of DCVAE to our modeling approach, which leverages the capabilities of causal flows and incorporates conditional prior. This greatly enhances the encoder’s ability to learn semantically meaningful and expressive representations.

Distributional robustness: To assess distributional robustness, we modify the controllable synthetic Pendulum dataset during training to inject spurious correlations between the target label and some spurious attributes. We choose *background_color* $\in \{blue(+), white(-)\}$ as a spurious feature. Specifically, in 80% of the examples, the target label and the spurious attribute are both positive or negative, while in 20% of the examples, they are opposite. For instance, in the manipulated training set, 80% of the positive examples in Pendulum are masked with a blue background. However, in the test set, we do not inject this correlation, resulting in a distribution shift. The results are summarized in Table 2.

The results include average and worst-case test accuracy, evaluating overall classification performance and distributional robustness. Worst-case accuracy identifies the group with the lowest accuracy among four groups categorized based on target and spurious binary labels. It often involves opposing spurious correlations compared to training data. The classifiers trained using DCVAE representations demonstrate significant superiority over all baseline models in both evaluation metrics. Notably, DCVAE experiences a smaller decrease in worst-case accuracy compared to average accuracy, indicating robustness to distributional shifts.

In the aforementioned experiments, we analyzed the reasons why our model outperforms DEAR, which are primarily twofold. First, DEAR uses an SCM prior to guide latent representation learning indirectly through loss minimization, whereas our model integrates causal flow directly into the VAE, using flow model characteristics to enhance latent representations. Second, DEAR employs a

Table 1. Test accuracy and sample efficiency of different models on Pendulum and CelebA datasets. Mean \pm standard deviations are included in the Table.

Model	Pendulum			CelebA		
	100(%)	All(%)	Sample Eff	100(%)	10000(%)	Sample Eff
DCVAE	99.00 \pm 0	99.43 \pm 0.34	99.57 \pm 0.34	81.00 \pm 1.73	81.54 \pm 1.76	99.34 \pm 0.27
DCVAE-SP	98.67 \pm 0.58	99.79 \pm 0.14	98.87 \pm 0.70	79.67 \pm 1.15	81.32 \pm 0.47	97.98 \pm 1.69
DEAR	88.00 \pm 0	88.55 \pm 0.04	98.63 \pm 1.33	61.00 \pm 3.60	68.50 \pm 0	89.05 \pm 5.26
β -VAE	98.67 \pm 1.15	99.59 \pm 0.07	98.94 \pm 0.92	62.33 \pm 5.69	68.49 \pm 0.02	91.01 \pm 8.28
β -TCVAE	97.67 \pm 1.15	99.38 \pm 0.48	98.27 \pm 0.79	75.33 \pm 3.21	78.72 \pm 4.93	95.83 \pm 4.10
VAE	98.33 \pm 0.58	99.48 \pm 0.39	98.72 \pm 0.37	60.33 \pm 2.89	68.50 \pm 0	88.08 \pm 4.21

Table 2. Distributional robustness of different models.

Model	TestAvg(%)	TestWorst(%)
DCVAE	97.83 \pm 1.18	94.70 \pm 3.41
DCVAE-SP	97.24 \pm 0.49	92.43 \pm 0.54
DEAR	80.40 \pm 0.47	64.50 \pm 2.67
β -VAE	96.48 \pm 2.06	90.05 \pm 5.44
β -TCVAE	96.57 \pm 1.33	90.27 \pm 3.74
VAE	95.14 \pm 3.46	88.81 \pm 5.44

fixed transformation function in its SCM prior, which may not align with the true causal function and affects performance. In contrast, our model utilizes causal flows, leveraging the benefits of autoregressive flows to adaptively learn superior transformation functions and improve VAE’s generative capability.

6.3.3 Exploring the potential for learning the structure A . Apart from the aforementioned applications, DCVAE has the potential to learn true causal relationships between factors, despite the fact that it is not the primary focus of our work. As shown in Figure 6(a)-6(d), for Pendulum, when our model A adopts the full graph shown in Figure 7(a), though the corresponding A is initialized randomly around 0, it gradually approaches the true causal structure during the training process. If we apply a threshold and prune edges in the causal graph, we obtain Figure 6(e), which corresponds to the true causal structure depicted in Figure 2(a). At this point, only four positions in matrix A are relatively large non-zero values, indicating accurate causal relationships. For the experiments conducted on CelebA dataset, please refer to Appendix B. This preliminary result suggests that our model has the potential to learn causal structures even without relying on a Structural Causal Model (SCM) [35, 49], inspiring us to explore this topic further in future research.

7 CONCLUSION AND POINTS OF FUTURE RESEARCH

In this paper, we focus on addressing the significant challenge of learning causal disentangled representations using VAE when the underlying generative factors are causally related. We propose the Disentangled Causal Variational Auto-Encoder (DCVAE), which leverages causal flows to integrate the causal structure information of generative factors into the model. Empirical results, including quantitative and qualitative experiments on synthetic and real-world datasets, validate our method’s success in learning causal disentangled representations and generating counterfactual outputs.

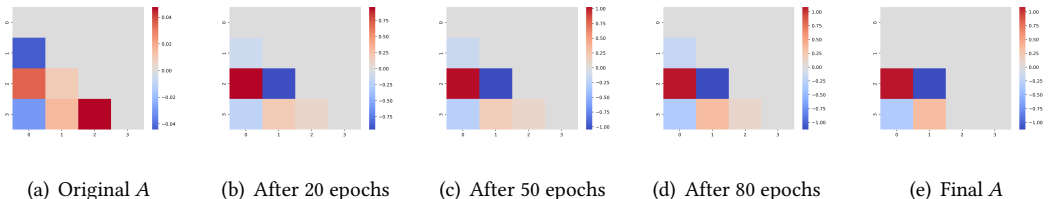


Fig. 6. The learned weighted adjacency matrix A given the causal ordering on Pendulum. (a)-(d) illustrate the changes in A as the training progresses. (e) represents A after edge pruning.

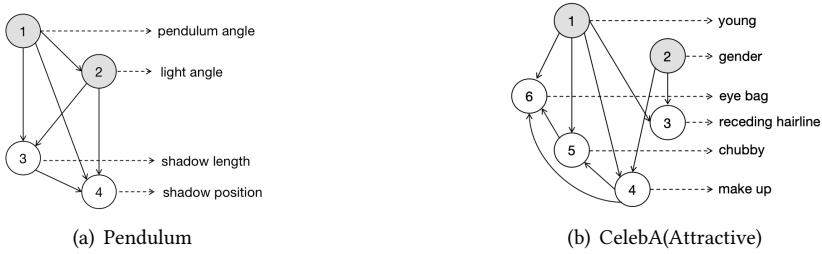


Fig. 7. Super-graph of Pendulum and CelebA(Attractive).

Future research directions present several opportunities. First, there is potential to extend this approach to model causal relationships among a broader set of generative factors, which is particularly relevant in the context of big data. Currently, our work offers a framework-based approach in this regard. Second, future studies could explore alternative forms of supervised information for disentanglement learning, as well as investigate weakly supervised or unsupervised methods to achieve causal disentangled representations within the flow model framework. Finally, a deeper exploration of the inherent structure of data could facilitate the learning of low-dimensional causal disentangled representations. Additionally, applying these representations to areas such as video generation presents a promising research direction.

ACKNOWLEDGMENTS

This work was funded by the National Nature Science Foundation of China under Grant No. 12320101001 and 12071428.

REFERENCES

- [1] SeungHwan An, Kyungwoo Song, and Jong-June Jeon. 2023. Causally disentangled generative variational autoencoder. In *ECAI 2023*. IOS Press, 93–100.
- [2] Yoshua Bengio, Aaron Courville, and Pascal Vincent. 2013. Representation learning: A review and new perspectives. *IEEE transactions on pattern analysis and machine intelligence* 35, 8 (2013), 1798–1828.
- [3] Diane Bouchacourt, Ryota Tomioka, and Sebastian Nowozin. 2018. Multi-level variational autoencoder: Learning disentangled representations from grouped observations. In *Proceedings of the AAAI Conference on Artificial Intelligence*, Vol. 32(1).
- [4] Johann Brehmer, Pim De Haan, Phillip Lippe, and Taco S Cohen. 2022. Weakly supervised causal representation learning. *Advances in Neural Information Processing Systems* 35 (2022), 38319–38331.
- [5] Simon Buchholz, Goutham Rajendran, Elan Rosenfeld, Bryon Aragam, Bernhard Schölkopf, and Pradeep Ravikumar. 2024. Learning linear causal representations from interventions under general nonlinear mixing. *Advances in Neural Information Processing Systems* 36 (2024).
- [6] Christopher P Burgess, Irina Higgins, Arka Pal, Loic Matthey, Nick Watters, Guillaume Desjardins, and Alexander Lerchner. 2018. Understanding disentangling in β -VAE. *arXiv preprint arXiv:1804.03599* (2018).
- [7] Ricky TQ Chen, Xuechen Li, Roger B Grosse, and David K Duvenaud. 2018. Isolating sources of disentanglement in variational autoencoders. *Advances in neural information processing systems* 31 (2018).
- [8] Emilien Dupont. 2018. Learning disentangled joint continuous and discrete representations. *Advances in Neural Information Processing Systems* 31 (2018).
- [9] Cian Eastwood and Christopher KI Williams. 2018. A framework for the quantitative evaluation of disentangled representations. In *International conference on learning representations*.
- [10] Amulya Gupta and Zhu Zhang. 2023. Neural Topic Modeling via Discrete Variational Inference. *ACM Transactions on Intelligent Systems and Technology* 14, 2 (2023), 1–33.
- [11] Jiawei He, Yu Gong, Joseph Marino, Greg Mori, and Andreas Lehrmann. 2018. Variational autoencoders with jointly optimized latent dependency structure. In *International conference on learning representations*.

- [12] Irina Higgins, Loic Matthey, Arka Pal, Christopher Burgess, Xavier Glorot, Matthew Botvinick, Shakir Mohamed, and Alexander Lerchner. 2017. beta-vae: Learning basic visual concepts with a constrained variational framework. In *International conference on learning representations*.
- [13] Haruo Hosoya. 2019. Group-based learning of disentangled representations with generalizability for novel contents. In *Proceedings of the 28th International Joint Conference on Artificial Intelligence (Macao, China) (IJCAI'19)*. 2506–2513.
- [14] Jun-Ting Hsieh, Bingbin Liu, De-An Huang, Li F Fei-Fei, and Juan Carlos Niebles. 2018. Learning to decompose and disentangle representations for video prediction. *Advances in neural information processing systems* 31 (2018).
- [15] Chin-Wei Huang, David Krueger, Alexandre Lacoste, and Aaron Courville. 2018. Neural autoregressive flows. In *International Conference on Machine Learning*. PMLR, 2078–2087.
- [16] Aapo Hyvarinen and Hiroshi Morioka. 2016. Unsupervised feature extraction by time-contrastive learning and nonlinear ica. *Advances in neural information processing systems* 29 (2016).
- [17] Tongyao Jia, Jiafeng Li, Li Zhuo, and Jing Zhang. 2024. Self-guided disentangled representation learning for single image dehazing. *Neural Networks* 172 (2024), 106107.
- [18] Ilyes Khemakhem, Diederik Kingma, Ricardo Monti, and Aapo Hyvarinen. 2020. Variational autoencoders and nonlinear ica: A unifying framework. In *International Conference on Artificial Intelligence and Statistics*. PMLR, 2207–2217.
- [19] Ilyes Khemakhem, Ricardo Monti, Robert Leech, and Aapo Hyvarinen. 2021. Causal autoregressive flows. In *International conference on artificial intelligence and statistics*. PMLR, 3520–3528.
- [20] Hyunjik Kim and Andriy Mnih. 2018. Disentangling by factorising. In *International Conference on Machine Learning*. PMLR, 2649–2658.
- [21] Minyoung Kim, Yuting Wang, Pritish Sahu, and Vladimir Pavlovic. 2019. Relevance factor vae: Learning and identifying disentangled factors. *arXiv preprint arXiv:1902.01568* (2019).
- [22] Durk P Kingma, Tim Salimans, Rafal Jozefowicz, Xi Chen, Ilya Sutskever, and Max Welling. 2016. Improved variational inference with inverse autoregressive flow. *Advances in neural information processing systems* 29 (2016).
- [23] Diederik P Kingma and Max Welling. 2014. Auto-encoding variational bayes. In *International conference on learning representations*.
- [24] Murat Kocaoglu, Christopher Snyder, Alexandros G Dimakis, and Sriram Vishwanath. 2018. Causalgan: Learning causal implicit generative models with adversarial training. In *International conference on learning representations*.
- [25] Abhishek Kumar, Prasanna Sattigeri, and Avinash Balakrishnan. 2018. Variational inference of disentangled latent concepts from unlabeled observations. In *International conference on learning representations*.
- [26] Simon Leglaive. 2022. A Multimodal Dynamical Variational Autoencoder for Audiovisual Speech Representation Learning. In *Proceedings of the 1st International Workshop on Methodologies for Multimedia*. 3–3.
- [27] Phillip Lippe, Sara Magliacane, Sindy Löwe, Yuki M Asano, Taco Cohen, and Stratis Gavves. 2022. Citris: Causal identifiability from temporal intervened sequences. In *International Conference on Machine Learning*. PMLR, 13557–13603.
- [28] Ziwei Liu, Ping Luo, Xiaogang Wang, and Xiaoou Tang. 2015. Deep learning face attributes in the wild. In *Proceedings of the IEEE international conference on computer vision*. 3730–3738.
- [29] Francesco Locatello, Stefan Bauer, Mario Lucic, Gunnar Raetsch, Sylvain Gelly, Bernhard Schölkopf, and Olivier Bachem. 2019. Challenging common assumptions in the unsupervised learning of disentangled representations. In *International conference on machine learning*. PMLR, 4114–4124.
- [30] Francesco Locatello, Ben Poole, Gunnar Rätsch, Bernhard Schölkopf, Olivier Bachem, and Michael Tschannen. 2020. Weakly-supervised disentanglement without compromises. In *International Conference on Machine Learning*. PMLR, 6348–6359.
- [31] Jianxin Ma, Chang Zhou, Peng Cui, Hongxia Yang, and Wenwu Zhu. 2019. Learning disentangled representations for recommendation. *Advances in neural information processing systems* 32 (2019).
- [32] Shanlei Mu, Yaliang Li, Wayne Xin Zhao, Siqing Li, and Ji-Rong Wen. 2021. Knowledge-guided disentangled representation learning for recommender systems. *ACM Transactions on Information Systems (TOIS)* 40, 1 (2021), 1–26.
- [33] George Papamakarios, Eric Nalisnick, Danilo Jimenez Rezende, Shakir Mohamed, and Balaji Lakshminarayanan. 2021. Normalizing flows for probabilistic modeling and inference. *The Journal of Machine Learning Research* 22, 1 (2021), 2617–2680.
- [34] Judea Pearl. 2009. *Causality*. Cambridge university press.
- [35] Judea Pearl et al. 2000. Models, reasoning and inference. *Cambridge, UK: CambridgeUniversityPress* 19, 2 (2000).
- [36] Abbavaram Gowtham Reddy, Vineeth N Balasubramanian, et al. 2022. On causally disentangled representations. In *Proceedings of the AAAI Conference on Artificial Intelligence*. 8089–8097.
- [37] Danilo Rezende and Shakir Mohamed. 2015. Variational inference with normalizing flows. In *International conference on machine learning*. PMLR, 1530–1538.
- [38] Bernhard Schölkopf. 2022. Causality for machine learning. In *Probabilistic and Causal Inference: The Works of Judea Pearl*. 765–804.

- [39] Yuanlong Shao, Yuan Zhou, and Deng Cai. 2011. Variational inference with graph regularization for image annotation. *ACM Transactions on Intelligent Systems and Technology (TIST)* 2, 2 (2011), 1–21.
- [40] Xinwei Shen, Furui Liu, Hanze Dong, Qing Lian, Zhitang Chen, and Tong Zhang. 2022. Weakly Supervised Disentangled Generative Causal Representation Learning. *Journal of Machine Learning Research* 23 (2022), 1–55.
- [41] Rui Shu, Yining Chen, Abhishek Kumar, Stefano Ermon, and Ben Poole. 2019. Weakly supervised disentanglement with guarantees. *arXiv preprint arXiv:1910.09772* (2019).
- [42] Casper Kaae Sønderby, Tapani Raiko, Lars Maaløe, Søren Kaae Sønderby, and Ole Winther. 2016. Ladder variational autoencoders. *Advances in neural information processing systems* 29 (2016).
- [43] Chandler Squires, Anna Seigal, Salil S Bhate, and Caroline Uhler. 2023. Linear causal disentanglement via interventions. In *International Conference on Machine Learning*. PMLR, 32540–32560.
- [44] Raphael Suter, Djordje Miladinovic, Bernhard Schölkopf, and Stefan Bauer. 2019. Robustly disentangled causal mechanisms: Validating deep representations for interventional robustness. In *International Conference on Machine Learning*. PMLR, 6056–6065.
- [45] Frederik Träuble, Elliot Creager, Niki Kilbertus, Francesco Locatello, Andrea Dittadi, Anirudh Goyal, Bernhard Schölkopf, and Stefan Bauer. 2021. On disentangled representations learned from correlated data. In *International Conference on Machine Learning*. PMLR, 10401–10412.
- [46] Xin Wang, Hong Chen, and Wenwu Zhu. 2023. Disentangled Representation Learning for Multimedia. In *Proceedings of the 31st ACM International Conference on Multimedia*. 9702–9704.
- [47] Antoine Wehenkel and Gilles Louppe. 2021. Graphical normalizing flows. In *International Conference on Artificial Intelligence and Statistics*. PMLR, 37–45.
- [48] Dingkan Yang, Shuai Huang, Haopeng Kuang, Yangtao Du, and Lihua Zhang. 2022. Disentangled representation learning for multimodal emotion recognition. In *Proceedings of the 30th ACM International Conference on Multimedia*. 1642–1651.
- [49] Mengyue Yang, Furui Liu, Zhitang Chen, Xinwei Shen, Jianye Hao, and Jun Wang. 2021. Causalvae: Disentangled representation learning via neural structural causal models. In *Proceedings of the IEEE/CVF conference on computer vision and pattern recognition*. 9593–9602.
- [50] Hangbin Zhang, Raymond K Wong, and Victor W Chu. 2021. Hybrid Variational Autoencoder for Recommender Systems. *ACM Transactions on Knowledge Discovery from Data (TKDD)* 16, 2 (2021), 1–37.

A EXPERIMENTAL DETAILS

We present the network architecture and hyperparameters used in our experiments. The network structures of encoder and decoder are presented in Table A.1. The encoder’s output, i.e., *mean* and *log variance*, share parameters except for the final layer. A single-layer causal flow implemented by an MLP implementation is used for fitting the posterior distribution, and a causal weight matrix A is added in a manner inspired by Wehenkel and Louppe [47]. Since the original encoder output z has already learned the information from x , we only input the z into the flow.

The decoder’s output is resized to generate pixel values for a three-channel color image. We train the model using the Adam optimizer and all the training parameters are shown in Table A.2. Although we cannot guarantee finding the optimal solution in the experiments, the empirical results still demonstrate the excellent performance of our model.

Table A.1. Architecture for the Encoder and Decoder in DCVAE ($d = 4$ for Pendulum and $d = 100$ for CelebA).

Encoder	Decoder
-	Input $\tilde{z} \in \mathbb{R}^d$
3×3 conv, MaxPool, 8 SELU, stride 1	FC, 256 SELU
3×3 conv, MaxPool, 16 SELU, stride 1	FC, 16×12×12 SELU
3×3 conv, MaxPool, 32 SELU, stride 1	2×2 conv, 32 SELU, stride 1
3×3 conv, MaxPool, 64 SELU, stride 1	2×2 conv, 64 SELU, stride 1
3×3 conv, MaxPool, 8 SELU, stride 1	2×2 conv, 128 SELU, stride 1
FC 256×2	FC, 3×64×64 Tanh

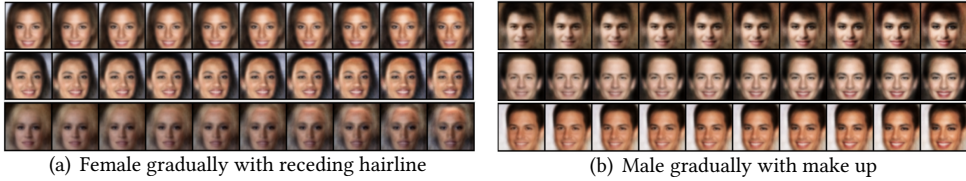


Fig. B.1. Sample from interventional distributions.

B ADDITIONAL RESULTS

B.1 Samples from interventional distributions

In Section 6.3.1, we describe the capability of our model to perform interventions by generating new images that do not exist in the dataset. Specifically, our model utilizes causal flows to sample from the interventional distributions, even though the model is trained on observational data. The steps for intervening on one factor are explained in section 6.3.1, and the same applies to intervening on multiple factors. As depicted in Figure 1(a), we intervene on the values of two factors by fixing gender as female and gradually adjusting the value of receding hairline. This produces a series of images showing women with a gradually receding hairline. Furthermore, as shown in Figure 1(b), we intervene on gender and makeup, generating a series of images of men with gradually applied makeup. These images are not commonly found or may not even exist in the training data, highlighting the ability of our model to sample from interventional distributions.

B.2 Learning of causal structure

DCVAE has the potential to learn causal structure between underlying factors, even though our work does not specifically focus on this aspect, and it does not use the Structural Causal Model (SCM) framework. Here we present the learning process of the adjacency weight matrix A , whose super-graph is shown in Figure 7. Figure B.2 shows the learning process of CelebA (Attractive). If we set a threshold of 0.25, i.e., considering edges in the causal graph smaller than the threshold as non-existing, we can obtain Figure 2(e). Our observation indicates that DCVAE effectively eliminates

Table A.2. Hyperparameters of DCVAE.

Parameters	Values (Pendulum)	Values (CelebA)
Batch size	128	128
Epoch	801	101
Latent dimension	4	100
σ	0.1667	0.1667
β_{sup}	8	5
β_1	0.2	0.2
β_2	0.999	0.999
ϵ	1e-8	1e-8
Learning rate of Encoder	5e-5	3e-4
Learning rate of Causal Flow	5e-5	3e-4
Learning rate of A	1e-3	1e-3
Learning rate of Conditional prior	5e-5	3e-4
Learning rate of Decoder	5e-5	3e-4

a significant portion of redundant variables and ultimately achieves a nearly accurate graph. This suggests the potential for further improvements in causal discovery through future research work.

B.3 Examining Causal Disentangled Representations

To verify whether our model has learned causal disentangled representations, we consider two types of intervention operations: the "traverse" operation and the "intervention" operation introduced in section 6.3.1. We present the experimental results of DCVAE on CelebA(Attractive) in Figure B.3 and the results of baseline models on three datasets in Figure B.4, B.5, and B.6.

B.4 Do Remaining Latent Variables Contain Useful Information about the underlying factors we we focus on?

We further conducted experiments to measure the influence of the remaining $m - d$ dimensions on the generated images in the CelebA dataset. As shown in Figure B.7, we measured the maximal information coefficient (MIC) and the total information coefficient (TIC) between the learned representations and the ground truth concept labels in the CelebA (Attractive) and CelebA (Smile) datasets. In these experimental settings, with $d=100$ and $m=6$, the first six units in the latent variable layer correspond to the six factors. From the figures, it is clear that the remaining 94 latent variable units contain almost no information about the generative factors we focus on. Therefore, the nature of these remaining latent variables ensures that the generation of counterfactual images can guarantee causal disentangled representation.

C REFLECTIONS ON DISENTANGLEMENT METRICS

Numerous disentanglement studies propose their own metrics, such as the β -VAE [12], FactorVAE [20], Mutual Information Gap (MIG) [7], and DCI [9]. A comprehensive review of these metrics can be found in Locatello et al. [29]. However, these metrics are typically limited to scenarios where generative factors are independent and do not extend to cases with factor correlations. For instance, the MIG score evaluates the normalized gap in mutual information between the highest and second-highest coordinates in $\bar{E}(\mathbf{x}, \mathbf{u})$. In cases where ξ_1 is correlated with ξ_2 , and a disentangled representation aligns each factor with one coordinate (i.e., $\bar{E}_1(\mathbf{x}, \mathbf{u}) = r_1(\xi_1)$ and $\bar{E}_2(\mathbf{x}, \mathbf{u}) = r_1(\xi_2)$), both coordinates will exhibit significant mutual information with their respective factors, leading to a minimal gap. Consequently, such a representation yields a low MIG score despite being properly disentangled. Metrics for causal disentanglement remain scarce and have limitations. Shen et al. [40] proposed a metric based on FactorVAE, which is the most suitable for our model compared to others like IRS [44] and (UC and GC) [36], which assume conditional independence. However, Kim et al. [21] demonstrated that this metric is not entirely reliable. In

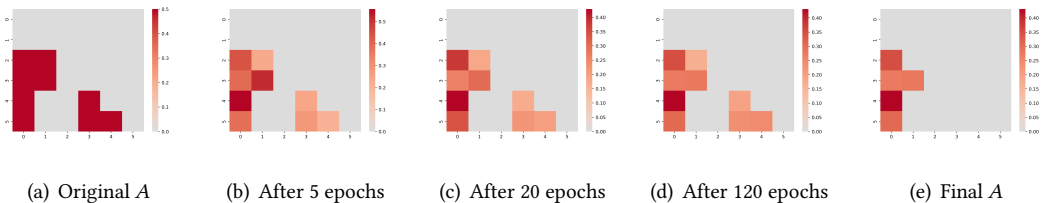


Fig. B.2. The learned weighted adjacency matrix A given a super-graph on CelebA(Attractive). (a)-(d) illustrate the changes in A as the training progresses. (e) represents A after edge pruning.



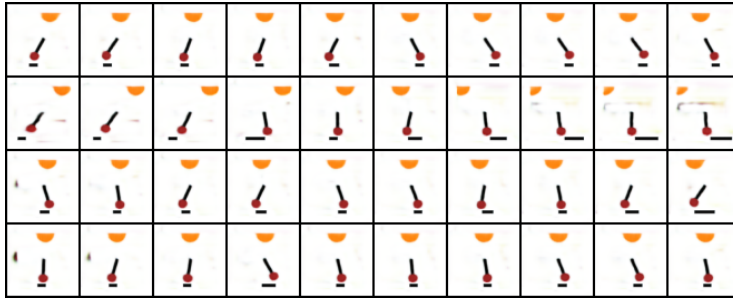
(a) Traversal of DCVAE on CelebA(Attractive)

(b) Intervention of DCVAE on CelebA(Attractive)

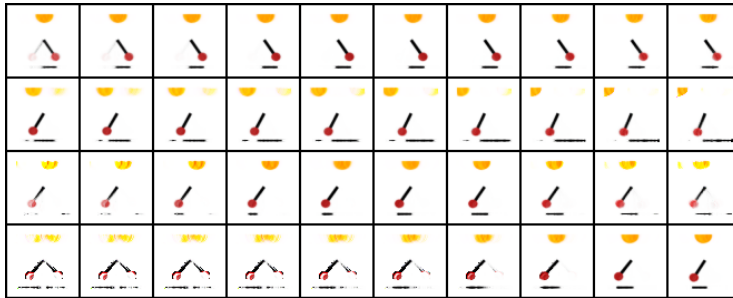
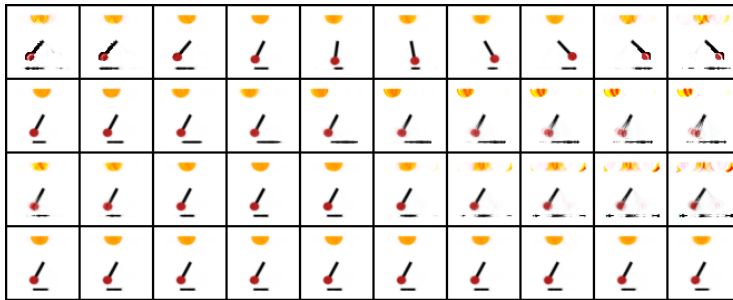
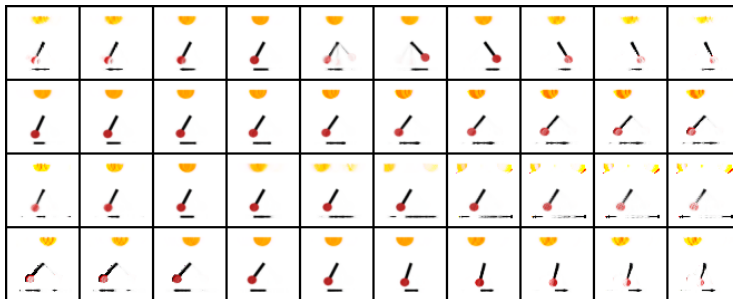
Fig. B.3. Results of the DCVAE model under two types of interventions on CelebA(Attractive). Each row corresponds to one factor, in the same order as in Figure 2(b). We observe that our model achieves disentanglement, and when intervening on the causal variables, it affects the effect variables, while the opposite is not true.

our experiments, FactorVAE scores [40] for models such as DCVAE, VAE, β -TCVAE, β -VAE, and DEAR were all 0.50, with DEAR scoring 0.28. These results suggest that, at minimum, our model outperforms the latest models like DEAR in causal disentanglement, though the FactorVAE metric has clear limitations. Therefore, to provide a more robust quantitative assessment, we conduct experiments on downstream tasks, where our model's superiority is evident both quantitatively and qualitatively.

Received 20 February 2007; revised 12 March 2009; accepted 5 June 2009



(a) DEAR

(b) β -VAE(c) β -TCVAE

(d) VAE

Fig. B.4. Traverse results of four baseline models on Pendulum. We observe that changing one factor may result in changes in multiple factors, or no changes in any factor, such as the shadow length in the β -TCVAE. Therefore, their representations are all entangled on Pendulum.

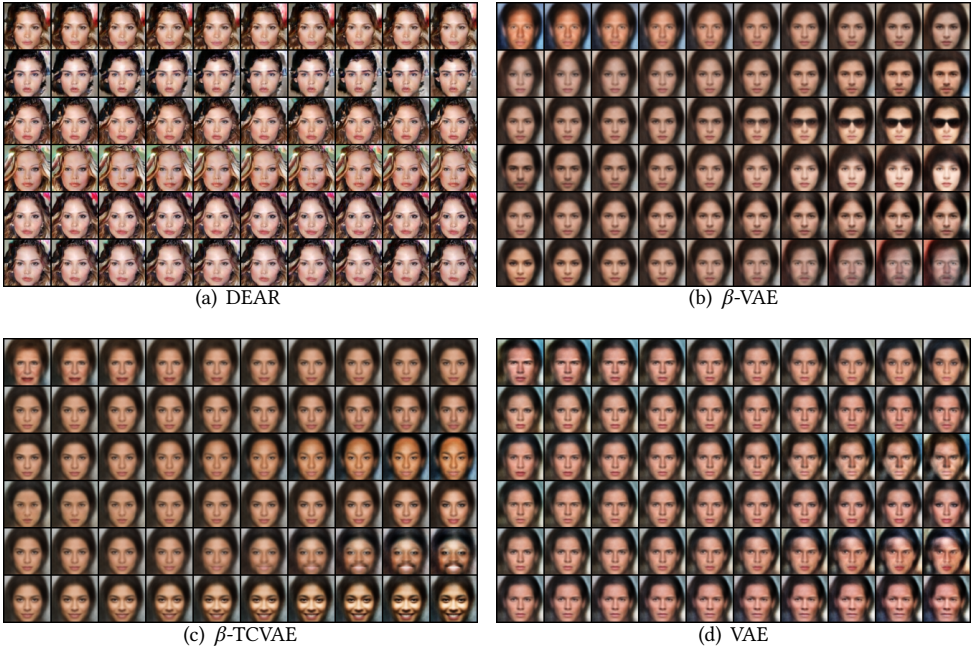


Fig. B.5. Traverse results of four baseline models on CelebA(Attractive).

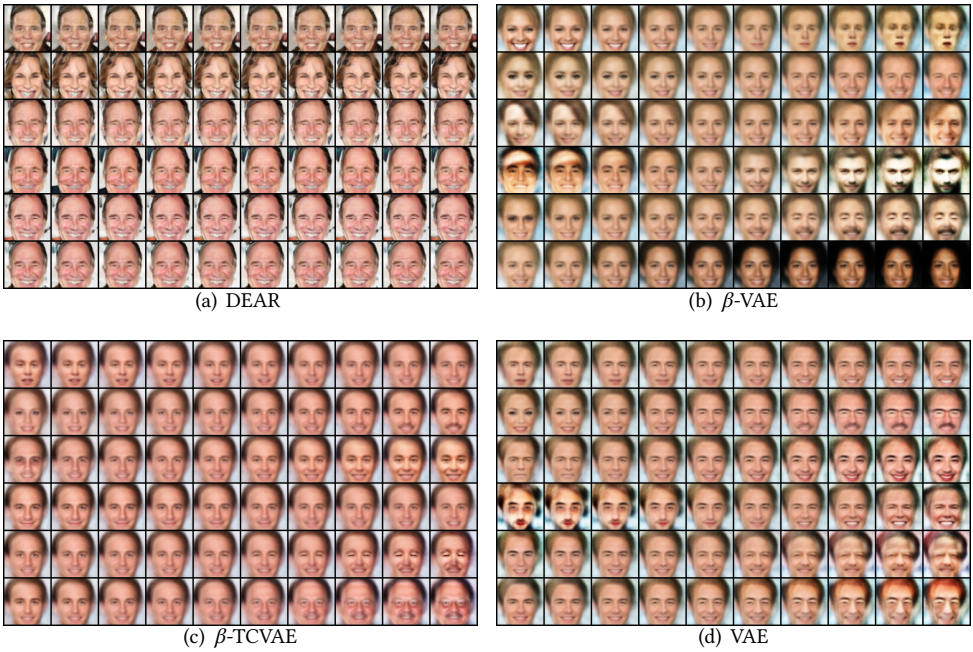


Fig. B.6. Traverse results of four baseline models on CelebA(Smile).

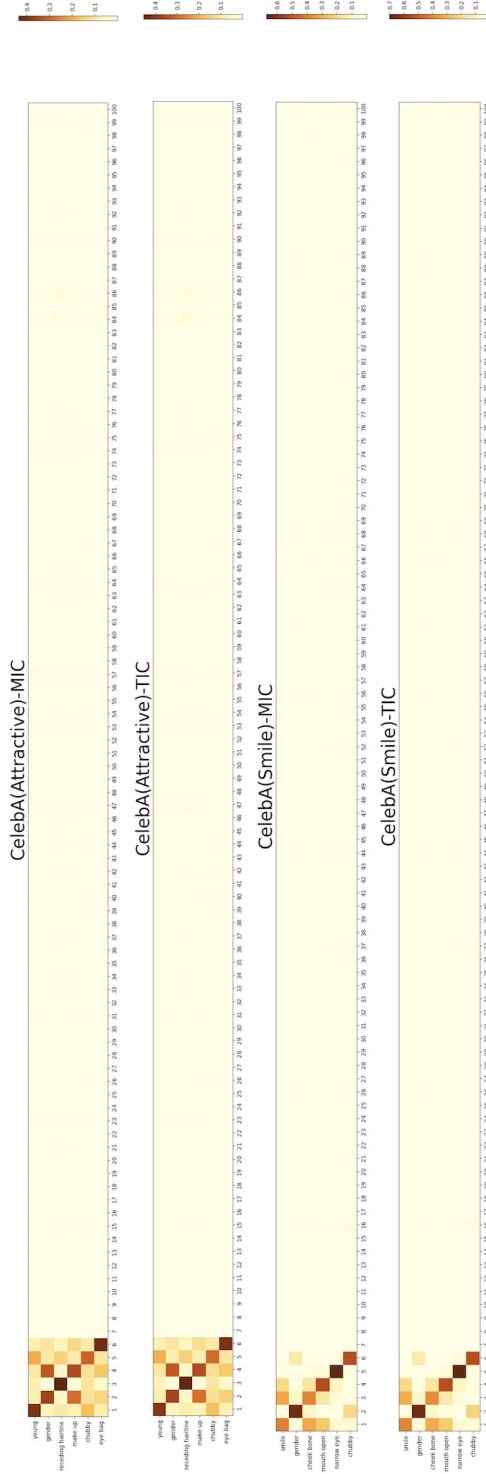


Fig. B.7. The mutual information (MIC/TIC) between the learned representation and the ground truth concept labels on the CelebA (Attractive) and CelebA (Smile) datasets.